Magnetic Properties of High-Pressure Phases *RE*Si$_3$

Ulrich Schwarz[#], Teuta Neziraj, Alim Ormeci, Lev Akselrud, Ulrich Burkhardt, Yuri Grin and Steffen Wirth[†]

Rare-earth metal silicides *RE*Si$_3$ (*RE* = Tb, Dy, Er, and Tm) with YbSi$_3$-type crystal structure exhibit Curie-Weiss paramagnetic behavior above their respective Néel temperatures T_N and antiferromagnetic ordering below T_N. The values of T_N follow a de Gennes scaling and hence, the coupling of the magnetic moments is likely mediated by the so-called RKKY interaction, i.e. via the conduction electrons. Isotypic SmSi$_3$ exhibits van Vleck paramagnetic behavior evidencing partially filled electronic states.

At ambient pressure, the silicon-richest phases of rare-earth metals are compounds *RE*Si$_{2-x}$ with defects in the silicon framework. By performing high-pressure high-temperature synthesis, phases like *M*Si$_3$ [1] or *M*Si$_5$ [2] are obtained. Here, compounds *M*Si$_3$ are of special interest as these form isotypic atomic arrangements for a variety of metals realizing different oxidation states, e.g., $M = Ca^{2+}$ and $M = Y^{3+}$; Lu^{3+} [CMS_01_Schwarz], [1]. For studying this set of intriguing compounds systematically, a series of new representatives *RE*Si$_3$ (*RE* = Sm – Tm) is synthesized at extreme conditions, i.e., high pressures and temperatures [3, 4, 5]. In the present work, we report on synthesis, crystal structure, chemical bonding and magnetic properties of these new binary silicon compounds.

Crystal structure and electronic properties

Applying high pressure of 9.5 GPa on precursor mixtures of *RE*Si$_{2-x}$ and Si at elevated temperatures in the range between 823 and 923 K yields new phases *RE*Si$_3$ for *RE* = Sm, Gd, Tb, Dy, Er, Tm. The products are quenched to ambient pressure and exhibit grayish metallic luster. At ambient conditions and in the inert atmosphere of glove boxes, the phases are metastable for several months. The similarity of the observed X-ray powder diffraction patterns indicates that the new compounds realize YbSi$_3$-type [6] crystal structures (space group *I*4/*mmm*). The chemical compositions of the synthesis products are characterized by energy dispersive and wavelength-dispersive X-ray spectroscopy. Except for SmSi$_{3-x}$, the analyses reveal ratios of *RE* metal to Si that are compatible with a composition of 1:3. In addition, the constitution of the terbium compound is verified by chemical analysis showing 24.96(2) at% Tb and 75.0(7) at% Si. Finally, contamination of the phases by hydrogen, oxygen and nitrogen is investigated using the example of the erbium compound. The measurements reveal only minor contaminations, the content of H_2 is below the detection limit. Detailed metallographic investigation of the samarium products with a nominal composition of $Sm_{25}Si_{75}$ result in the composition $Sm_{25.6(1)}Si_{74.4(1)}$. This finding motivated studies by X-ray single-crystal diffraction disclosing a small silicon deficit causing a defect structure of larger particles [CMS_01_Schwarz].

The atomic arrangement comprises two-dimensional silicon segments separated by twelve-coordinated rare-earth metal atoms. The intricate Si layers comprise dumbbells

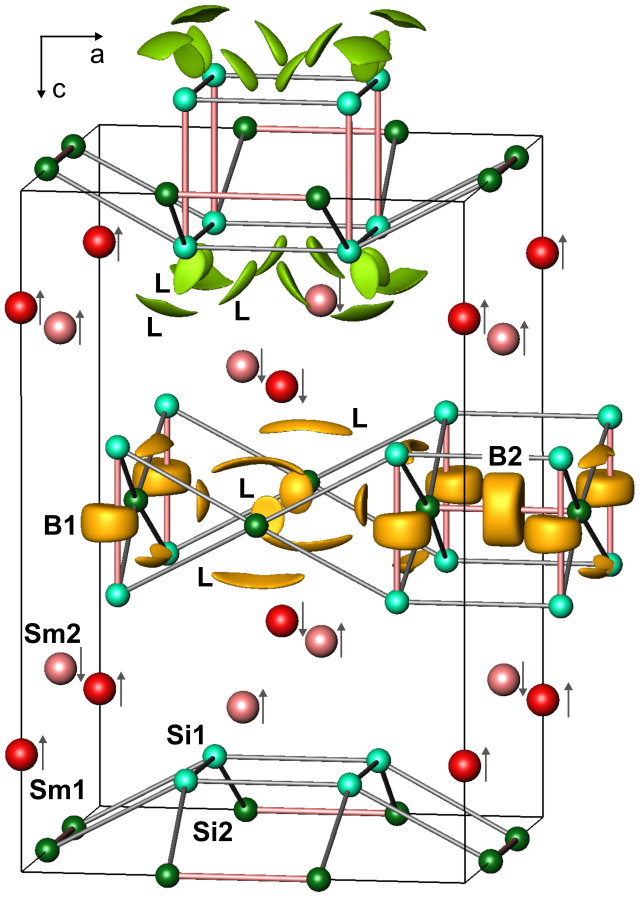

Fig. 1: Crystal structure of compounds RESi$_3$ (RE = Sm, Gd, Tb, Dy, Ho, Er, Tm) and chemical bonding of SmSi$_3$. Orange isosurfaces indicate bonding attractors associated to covalent two-atomic (two-center) Si-Si bonds (labeled B1 and B2, respectively). The green isosurfaces indicate lone pair-like attractors close to the Si1 atoms; the corresponding attractors of Si2 are shown in gold (labels L). The magnetic structure computed for SmSi$_3$ with antiferromagnetic order is visualized by arrows. Computations are realized using the LSDA+U method and selecting the value U = 8 eV.

in orientations parallel and perpendicular to [001], i.e. the *c*-axis (Figure 1).

Comparison of unit cell volumes against atomic number for compounds $RESi_3$ (RE = Gd – Lu) show a monotonic decrease (Figure 2) except for $YbSi_3$. Such a trend is expected because of the lanthanide contraction of the rare-earth metal ions. The anomaly of $YbSi_3$ is in line with the preference of the rare-earth metal ytterbium for adopting the $4f^{14}$ configuration.

In order to investigate the chemical bonding [**CMS_04_Wagner**], a concerted topological analysis using the electron density combined with the electron-localizability indicator (ELI-D) is performed. The effective charges are close to the values reported earlier for isotypic $GdSi_3$ and amount to Sm1: +0.97, Sm2: +1.01, Si1: -0.32, and Si2: 0.35. Likewise, the basic features of the chemical bonding situation in $SmSi_3$ are very similar to those of $GdSi_3$. The homoatomic Si1–Si1 and Si2–Si2 bonds (B in Figure 1) contain 1.62 and 1.91 electrons, respectively. These values are in good agreement with typical values found for single bonds. The interaction Si1-Si1 is a pure two-center bond, while the bonding Si2-Si2 shows additional contributions from two Sm1 atoms (0.06 e^-).

There are three lone-pair (L in Figure 1) attractors per Si atom. The basin populations of those involving Si1 are Si1-Sm1-Sm2 with 0.81 e^-, Si1-Sm1-Sm2 with 0.79 e^-, and Si1-Sm2-Sm2-Sm1 with 1.96 electrons, summing up to the total number of 3.56 e^- for Si1, of which about 94% are provided by the silicon atom. The total Sm contributions for Si1 correspond to (0.04) e^- for the first two bonds and to (0.11) e^- for the third one. The attractors of the Si2 lone pairs exhibit the populations Si2-Sm2-Sm2 of 0.69 e^-, Si2-Si1-Sm1-Sm2 of 1.48 e^- and Si2-Si1-Sm1-Sm2 of 1.46 e^-. From the total of 3.63 e^-, the Si2 contributions amount to ~92%. The Sm contributes between (0.06) e^- and (0.04) e^-. The total numbers of electrons, 3.56 e^- and 3.63 e^-, agree well with the expected value for two lone pairs at each silicon atom. The finding of metal contributions, like those observed in the Si-Si basins, is attributed to the presence of strongly polar multiatomic bonds as were previously found in Zintl-phases and related compounds.

As an example for the rare-earth metal trisilicides, the electronic structure of $SmSi_3$ is investigated by LSDA and LSDA+U computations using the ideal $YbSi_3$-type crystal structure. Both techniques consistently indicate antiferromagnetic (AFM) coupling as the preferred long-range order (Figure 3), and both results are very close in energy. However, the optimal ordering schemes are different. The spins of neighboring Sm2 atoms, which exhibit the shortest Sm2 – Sm2 distances, are antiparallel in the LSDA+U result. The density of states at the Fermi level E_F corresponds to 10.56 states eV^{-1} $f.u.^{-1}$ for LSDA versus 1.48 states eV^{-1} $f.u.^{-1}$ in the LSDA+U case. The calculated spin magnetic moments for (Sm1, Sm2) amount to $\pm(5.73, 5.76)$ in LSDA, and $\pm(6.09, 6.09)$ in LSDA+U. It is typical for the LSDA method that the positioning of the f states near E_F gives rise to very high values of the DOS at E_F.

Assuming that LSDA+U is a more accurate approximation for the Sm $4f$ electrons, the electronic structure and chemical bonding features of $SmSi_3$ are analyzed using the results obtained by this method. In the calculated density of states, the Sm $4f$ states are located at around 1.5 eV having a total width of about 1 eV (Figure 3).

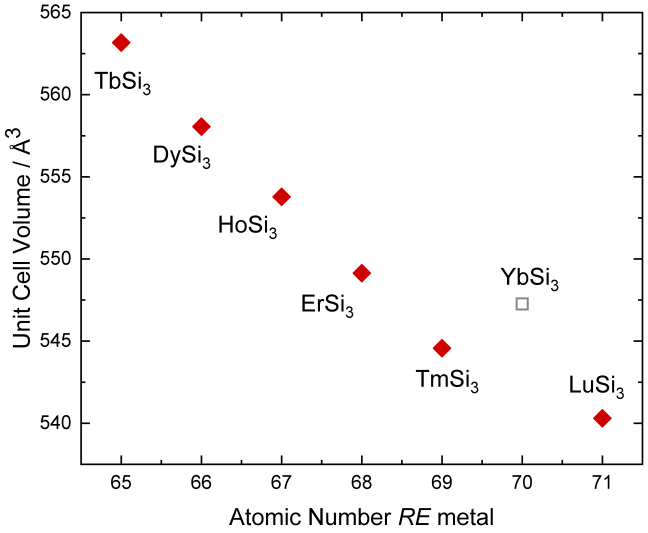

Fig. 2: Unit cell volumes of rare-earth metal trisilicides $RESi_3$. The continuous decrease for RE^{3+} reflects the lanthanoide contraction. The anomaly of the ytterbium compound is attributed to the realization of Yb^{2+}.

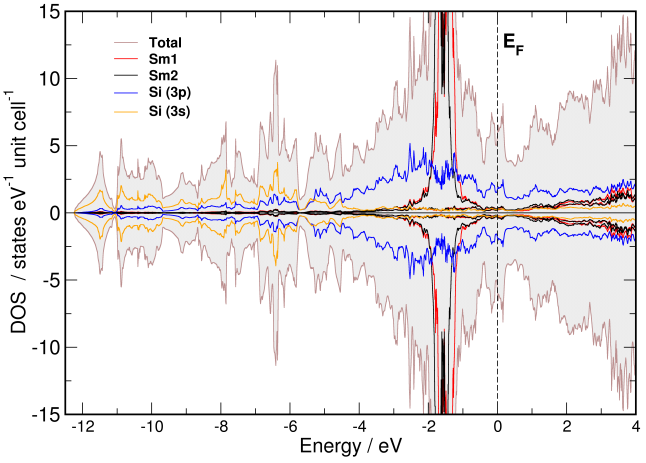

Fig. 3: Electronic density of states for $SmSi_3$ with antiferromagnetic arrangement of Sm spins. The upper curves represent the spin-up channel, the spin-down part is shown below.

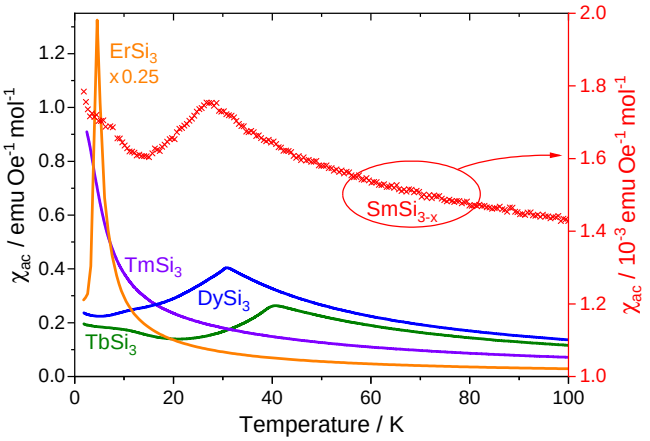

Fig. 4: Ac magnetic susceptibility $\chi_{ac}(T)$ of some $RESi_3$ compounds shown for temperatures from 1.8 to 100 K (measurements conducted up to 300 K). Note that $\chi_{ac}(T)$ of $ErSi_3$ has been multiplied by a factor of 0.25 for ease of comparison. Values of $\chi_{ac}(T)$ of $SmSi_{3-x}$, red crosses and right scale with prefactor 10^{-3}, are considerably smaller compared to the other $RESi_3$ compounds.

Between the bottom of the valence band (approximately 12.25 eV) and 5.70 eV, Si 3*s* contributions are more dominant than the Si 3*p* ones. Above 5.70 eV, Si 3*p* states clearly dominate as the contributions of the metal atoms, Sm 6*s*, 6*p* and 5*d*, are small.

Magnetic properties of *RE*Si$_3$

Magnetic ac susceptibility measurements $\chi_{\rm ac}(T)$ of some of the new phases $RESi_3$ are presented in Figure 4. $SmSi_3$ exhibits a value of $\chi_{\rm ac}$ which is about three orders of magnitude smaller compared to its sister compounds. This points to a severely different magnetic behavior of $SmSi_{3-x}$ and hence, this compound will be discussed separately.

Compounds with RE = Gd – Tm

In the paramagnetic state (i.e. at higher temperatures), $\chi_{\rm ac}(T)$ of the new phases $RESi_3$ with *RE* = Gd, Tb, Dy, Ho, Er and Tm [4, 5] can be well described by Curie-Weiss laws [7]

$$\chi_{\rm ac}(T) = \frac{N\mu_0\,\mu_{\rm eff}^2}{3k_{\rm B}(T-\theta)} \quad . \tag{1}$$

Here, θ is the paramagnetic Weiss temperature which is a measure of dominating ferromagnetic ($\theta > 0$) or antiferromagnetic ($\theta < 0$) interactions, N is the number of magnetic atoms and $\mu_{\rm eff}$ the effective magnetic moment. Fitting $\chi_{\rm ac}(T)$ to eq. 1 yields the parameters as summarized in Table 1. An exemplary fit for $GdSi_3$ is shown by the red line in Figure 5. The experimentally determined

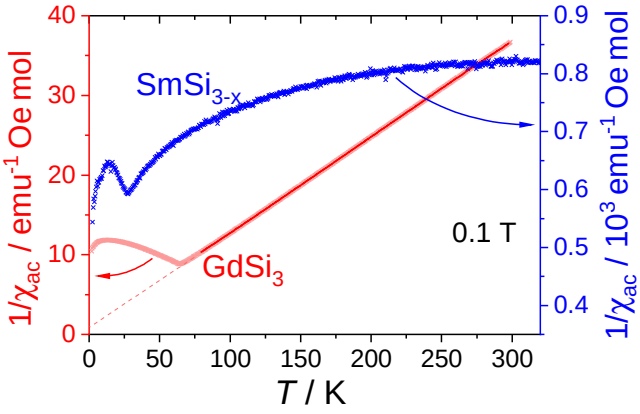

Fig. 5: Inverse magnetic susceptibility $1/\chi_{\rm ac}(T)$ of $GdSi_3$ (red and left scale) and $SmSi_{3-x}$ (blue and right). $\chi_{\rm ac}(T)$ measured at 0.1 T. Due to the small values of $\chi_{\rm ac}(T)$ of $SmSi_3$, the right scale is divided by 10^3.

values $\mu_{\rm eff}$ agree reasonably well with those of $\mu_{\rm theo}$ confirming the trivalent ground state of the respective *RE* ion. The Weiss temperatures are negative and small for all compounds pointing to weak antiferromagnetic interactions between the *RE* ions.

Since the $\chi_{ac}(T)$ of the $RESi_3$ compounds (except $SmSi_3$) nicely follow the Curie-Weiss law, a mean field approach can be applied, i.e. the interactions between magnetic moments can be described by an effective field proportional to the magnetization generated by the thermal average of the surrounding RE^{3+} moments. This magnetization and hence, the interactions can be calculated (apart from a proportionality constant) from the the total angular momentum J and the Landé factor g_J of the respective rare earth ion. Such an approach is usually applicable for *RE*-containing compounds since direct exchange interaction between $4f$ electrons is negligible. Moreover, we here assume a well-defined Hund´s rule ground state for J. Within the mean field approach, the Néel temperature $T_{\rm N}$ scales then with the magnitude of the interaction

$$\begin{aligned} T_{\rm N} &\propto G \\ G &= (g_J-1)^2 J(J+1) \end{aligned} \tag{2}$$

where G is the de Gennes factor. The applicability of de Gennes scaling for isostructural compounds with exclusive RE^{3+} magnetic moments has been investigated extensively in the literature, e.g. very recently for REV_6Sn_6 [8]. In Fig. 6, $T_{\rm N}$ is plotted against G for our series of $RESi_3$. Clearly, excellent scaling is observed. In case of $TmSi_3$ no indication for magnetic ordering is found down to the lowest measurement temperature of 2 K, in line with the expectations from the de Gennes scaling. Note that $YbSi_3$ is not included here because of the diamagnetic nature of its Yb^{2+} oxidation state.

Table 1: Electron configuration, Néel temperatures T_N, paramagnetic Weiss temperature θ and experimental and theoretical paramagnetic moments of the rare-earth ions for compounds $RESi_3$ (RE = Sm, Gd – Tm).

	config.	T_N K	θ K	μ_{eff} μ_B	μ_{theo} μ_B
$SmSi_{3-x}$	$^6H_{5/2}$	27	−0.58	0.34(20)	0.85
$GdSi_3$	$^8S_{7/2}$	64	−6.7	8.13(8)	7.94
$TbSi_3$	$^5F_6$	41(2)	−3.6	9.80	9.72
$DySi_3$	$^6H_{15/2}$	31	−3.5	10.62	10.65
$HoSi_3$	$^5I_8$	11	−4.1	10.87	10.6
$ErSi_3$	$^4I_{15/2}$	6	−4.4	9.21	9.58
$TmSi_3$	$^3H_6$	< 2	−15.0	8.09	7.56
error		±1	±0.5	±0.01	

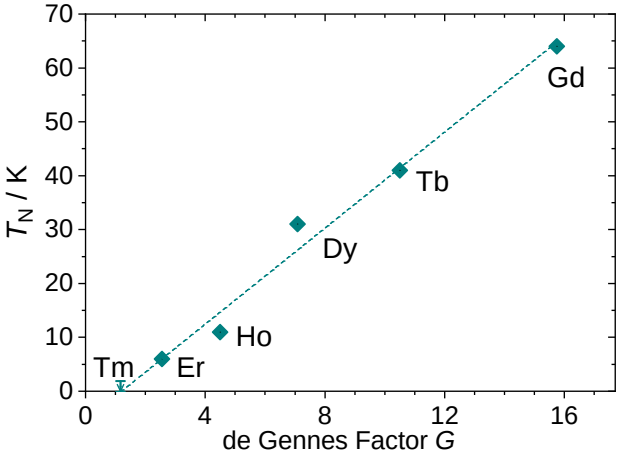

Fig. 6: Néel temperature T_N in dependence on the de Gennes factor G for different compounds $RESi_3$ (RE = Gd–Tm). The respective rare-earth element is indicated in the plot. Any possible magnetic ordering in $TmSi_3$ falls below the lowest measurement temperature of 2 K as marked by the small arrow.

The very good de Gennes scaling observed for our $RESi_3$ compounds has several implications. It readily points to an indirect coupling between the local RE^{3+} magnetic moments via polarization of the conduction electrons, i.e. towards Ruderman-Kittel-Kasuya-Yosida (RKKY) interaction. A quenching of the orbital moments in these materials can likely be excluded; only in case of $DySi_3$ some quenching toward a spin-only magnetic moment may be indicated [9]. More importantly, the applicability of the mean field approach underlying the de Gennes scaling points toward negligible influences of crystalline electric field (CEF) effects and anisotropic exchange on the magnetic properties of $RESi_3$ [9, 10].

The compound $SmSi_{3-x}$

As shown in Figure 4 and 5, the compound $SmSi_{3-x}$ exhibits a much smaller $\chi_{ac}(T)$ which also does not follow a Curie-Weiss law (see eq. 1) [3]. Intriguingly, at high temperatures an almost temperature-independent value of $\chi_{ac}(T)$ of order 10^{-3} emu Oe^{-1} mol^{-1} is observed, which is expected for Sm^{3+} ions [11, 12]. Such a behavior is indicative of van Vleck paramagnetism [7]. This contribution to the susceptibility arises if partially filled electronic states exist and hence, angular momentum states at higher energy can be excited. Typically, energy gap Δ between the ground state and the excited state(s) is so large that van Vleck contributions to $\chi_{ac}(T)$ can be ignored. The few exceptions here include Sm^{3+} and Eu^{3+} containing materials. Note that the van Vleck susceptibility χ_{vV} is independent of temperature for $\Delta \gg k_B T$ and hence, only susceptibility data at low enough temperature should be analyzed. Additionally, the small magnetic moments of Sm^{3+} ($\mu_{eff} = 0.85\mu_B$) can interact at low enough temperatures and give rise to a Curie-Weiss behaviour. Consequently, the measured $\chi_{ac}(T)$ at low temperatures contains both contributions: $\chi_{ac}(T) = \chi_{CW}(T) + \chi_{vV}$. Fitting our $\chi_{ac}(T)$ data within the range 2.4 K $\leq T \leq$ 13 K yields $\mu_{eff} = 0.34\mu_B$ and $\theta = -0.58$ K. Such a reduced value of μ_{eff} (cf. Table 1) is commonly observed in Sm^{3+} oxides and is indicative of crystalline electric field (CEF) effects.

The increasing value of $\chi_{ac}(T)$ above 13 K and the maximum at 27 K can then be explained by CEF effects. In Sm^{3+} ions, excited CEF levels with larger magnetic moment than the ground state can easily be occupied due to the relatively small energy Δ upon increasing temperature. By comparison to the pyrochlore $Sm_2Ti_2O_7$ [12, 13] we estimated Δ to amount to 3–4 meV.

The small magnetic moment of Sm^{3+} results in weak dipolar interactions between the ions and is reflected in the very small $\chi_{ac}(T)$ compared to the other rare earth trisilicides discussed above. Hence, magnetic ordering is expected only at very low temperatures, in line with the low-T χ_{ac} fitting range used above.

We also conducted measurements of the specific heat on $SmSi_{3-x}$ in magnetic fields of zero $\mu_0 H = 6$ T up to 80 K, which confirmed the above scenario [3]. Above T_N, these data can again nicely be compared to those of the Sm pyrochlores [11]. They also allow for a rough estimate of the magnetic contribution to the specific heat from which the magnetic entropy S_{mag} can be calculated by integration. Beyond the magnetic transition, $S_{mag} \sim 6$ J/(K mol_{Sm}) is in good agreement with the value $R \ln 2 = 5.76$ J/(K mol_{Sm}) expected for a Kramers doublet of Sm^{3+}.

References

[1] *Dumbbells of Five-Connected Silicon Atoms and Superconductivity in the Binary Silicides MSi_3 (M = Ca, Y, Lu)*, U. Schwarz, A. Wosylus, H. Rosner, W. Schnelle, A. Ormeci, K. Meier, A. Baranov, M. Nicklas, S. Leipe, C. J. Müller, and Y. Grin, J. Am. Chem. Soc. (2012) 13558, https://dx.doi.org/10.1021/ja3055194

[2] *Unusual Silicon Connectivities in the Binary Compounds $GdSi_5$, $CeSi_5$ and Ce_2Si_7*, A. Wosylus, K. Meier, Y. Prots, W. Schnelle, H. Rosner, U. Schwarz, and Y. Grin, Angew. Chem. Int. Ed. (2010) 9002, https://dx.doi.org/10.1002/anie.201003490

[3]* *Real Structure, Magnetism and Chemical Bonding in $SmSi_3$*, T. Neziraj, Y. Prots, W. Carrillo-Cabrera, A. Ormeci, S. Wirth, A. Fitch, U. Burkhardt, Y. Grin, and U. Schwarz, Eur. J. Inorg. Chem. (2024) e202300738, https://dx.doi.org/10.1002/ejic.202300738

[4]* *Gadolinium trisilicide – a paramagnetic representative of the $YbSi_3$ type series*, T. Neziraj, K. Meier-Kirchner, W. Schnelle, S. Wirth, Y. Grin, and U. Schwarz, Z. Naturforsch. B **77** (2022) 323, https://dx.doi.org/10.1515/znb-2022-0024

[5]* *Crystal Structure and Magnetic Properties of High-Pressure Phases $RESi_3$ (RE = Tb, Dy, Er, Tm)*, T. Neziraj, L. Akselrud, S. Wirth, and U. Schwarz, Z. Anorg. Allg. Chem. **649** (2023) e202300119, https://dx.doi.org/10.1002/zaac.202300119

[6] *Crystal structure of ytterbium trisilicide, $YbSi_3$*, A. Wosylus, Y. Prots, and U. Schwarz, Z. Kristallogr. NCS **226** (2011) 295, https://dx.doi.org/10.1524/ncrs.2011.0130

[7] *Tutorial: a beginner's guide to interpreting magnetic susceptibility data with the Curie-Weiss law*, S. Mugiraneza, and A. M. Hallas, Commun. Phys. **5** (2022) 95, https://dx.doi.org/10.1038/s42005-022-00853-y

[8] *Anisotropic magnetic property of single crystals RV_6Sn_6 (R = Y, Gd–Tm, Lu)*, J. Lee, and E. Mun, Phys. Rev. Mater. **6** (2022) 083401, https://dx.doi.org/10.1103/PhysRevMaterials.6.083401

[9] *Magnetic Characteristics of Laves Phases Containing Lanthanide Metals Combined with Nickel*, E. A. Skrabek, and W. E. Wallace, J. Appl. Phys. **34** (1963) 1356, https://dx.doi.org/10.1063/1.1729507

[10] *Magnetic-susceptibility and electrical-resistivity measurements on RPdSn (R = Ce–Yb) compounds*, D. T. Adroja, and S. K. Malik, Phys. Rev. B **45** (1992) 779, https://dx.doi.org/10.1103/PhysRevB.45.779

[11] *Manifestation of geometric frustration on magnetic and thermodynamic properties of the pyrochlores $Sm_2X_2O_7$ (X = Ti, Zr)*, S. Singh, S. Saha, S. K. Dhar, R. Suryanarayanan, A. K. Sood, and A. Revcolevschi, Phys. Rev. B **77** (2008) 054408, https://dx.doi.org/10.1103/PhysRevB.77.054408

[12] *Intermultiplet transitions and magnetic long-range order in Sm-based pyrochlores*, V. Peçanha-Antonio, E. Feng, X. Sun, D. Adroja, H. C. Walker, A. S. Gibbs, F. Orlandi, Y. Su, and T. Brückel, Phys. Rev. B **99** (2019) 134415, https://dx.doi.org/10.1103/PhysRevB.99.134415

[13] *Understanding Optical Absorption Spectra and Magnetic Behavior of a Wide Range of Samarium(III) Oxo-Compounds: Analysis of the Ligand-Field Effects*, N. Kannengießer, M. Jähnig, R. K. Kremer, and R. Glaum, Eur. J. Inorg. Chem. (2021) 1722, https://dx.doi.org/10.1002/ejic.202001115

[#] ulrich.schwarz@cpfs.mpg.de

[†] steffen.wirth@cpfs.mpg.de